

Beam-Target Helicity Asymmetry E in $K^+\Sigma^-$ Photoproduction on the Neutron

N. Zachariou,^{1,*} D. Watts,¹ J. Fleming,² A.V. Sarantsev,³ V.A. Nikonov,³ A. D'Angelo,^{22,34} M. Bashkanov,¹ C. Hanretty,^{38,44} T. Kageya,³⁸ F.J. Klein,⁹ M. Lowry,³⁸ H. Lu,⁴ A. Sandorfi,³⁸ X. Wei,³⁸ I. Zonta,³⁴ K.P. Adhikari,^{32,†} S. Adhikari,¹⁷ M.J. Amarian,³² G. Angelini,¹⁹ G. Asryan,⁴⁶ H. Atac,³⁷ L. Barion,²⁰ M. Battaglieri,^{38,21} I. Bedlinskiy,²⁸ F. Benmokhtar,¹⁴ A. Bianconi,^{41,24} A.S. Biselli,¹⁵ F. Bossù,¹⁰ S. Boiarinov,³⁸ W.J. Briscoe,¹⁹ W.K. Brooks,³⁹ D. Bulumulla,³² D.S. Carman,³⁸ J.C. Carvajal,¹⁷ G. Charles,^{10,‡} P. Chatagnon,²⁵ T. Chetry,²⁷ G. Ciullo,^{20,16} M. Contalbrigo,²⁰ N. Dashyan,⁴⁶ R. De Vita,²¹ A. Deur,³⁸ S. Diehl,¹² C. Djalali,^{31,36} R. Dupre,^{25,10,5} H. Egiyan,³⁸ M. Ehrhart,⁵ A. El Alaoui,^{39,5} P. Eugenio,¹⁸ S. Fegan,^{42,§} R. Fersch,^{11,45} A. Filippi,²³ G. Gavalian,^{38,32} N. Gevorgyan,⁴⁶ Y. Ghandilyan,⁴⁶ G.P. Gilfoyle,³³ W. Gohn,^{12,¶} R.W. Gothe,³⁶ K.A. Griffioen,⁴⁵ M. Guidal,²⁵ K. Hafidi,⁵ H. Hakobyan,^{39,46} M. Hattawy,³² D. Heddle,^{11,38} K. Hicks,³¹ M. Holtrop,²⁹ D.G. Ireland,⁴² B.S. Ishkhanov,³⁵ E.L. Isupov,³⁵ D. Jenkins,⁴³ H.S. Jo,^{26,25} K. Joo,¹² D. Keller,⁴⁴ M. Khachatryan,³² A. Khanal,¹⁷ M. Khandaker,^{30,**} C.W. Kim,¹⁹ W. Kim,²⁶ V. Kubarovskiy,³⁸ L. Lanza,²² M. Leali,^{41,24} P. Lenisa,²⁰ I. J. D. MacGregor,⁴² D. Marchand,²⁵ N. Markov,¹² V. Mascagna,^{40,24,††} B. McKinnon,⁴² V. Mokeev,^{38,35} E. Munevar,^{38,19} C. Munoz Camacho,²⁵ T. R. O'Connell,¹² M. Osipenko,²¹ A.I. Ostrovidov,¹⁸ M. Paolone,^{37,36} L.L. Pappalardo,²⁰ K. Park,³⁸ E. Pasyuk,³⁸ W. Phelps,¹¹ O. Pogorelko,²⁸ J. Poudel,³² J.W. Price,⁶ Y. Prok,^{32,11} A.J.R. Puckett,^{38,‡‡} B.A. Raue,^{17,38} M. Ripani,²¹ A. Rizzo,^{22,34} G. Rosner,⁴² C. Salgado,³⁰ A. Schmidt,¹⁹ R.A. Schumacher,⁸ U. Shrestha,³¹ D. Sokhan,^{42,25} N. Sparveris,³⁷ I.I. Strakovsky,¹⁹ S. Strauch,³⁶ J.A. Tan,²⁶ N. Tyler,³⁶ M. Ungaro,³⁸ L. Venturelli,^{41,24} H. Voskanyan,⁴⁶ E. Voutier,²⁵ M.H. Wood,⁷ J. Zhang,⁴⁴ and Z.W. Zhao^{13,44}

(The CLAS Collaboration)

¹University of York, York YO10 5DD, United Kingdom

²University of Edinburgh, Edinburgh EH9 3FD, United Kingdom

³Helmholtz-Institut fuer Strahlen- und Kernphysik, Universitaet Bonn, 53115 Bonn, Germany
National Research Centre Kurchatov Institute, Petersburg Nuclear Physics Institute, Gatchina, 188300 Russia

⁴University of Iowa, Iowa City, Iowa 52242

⁵Argonne National Laboratory, Argonne, Illinois 60439

⁶California State University, Dominguez Hills, Carson, CA 90747

⁷Canisius College, Buffalo, NY

⁸Carnegie Mellon University, Pittsburgh, Pennsylvania 15213

⁹Catholic University of America, Washington, D.C. 20064

¹⁰IRFU, CEA, Université Paris-Saclay, F-91191 Gif-sur-Yvette, France

¹¹Christopher Newport University, Newport News, Virginia 23606

¹²University of Connecticut, Storrs, Connecticut 06269

¹³Duke University, Durham, North Carolina 27708-0305

¹⁴Duquesne University, 600 Forbes Avenue, Pittsburgh, PA 15282

¹⁵Fairfield University, Fairfield CT 06824

¹⁶Universita' di Ferrara, 44121 Ferrara, Italy

¹⁷Florida International University, Miami, Florida 33199

¹⁸Florida State University, Tallahassee, Florida 32306

¹⁹The George Washington University, Washington, DC 20052

²⁰INFN, Sezione di Ferrara, 44100 Ferrara, Italy

²¹INFN, Sezione di Genova, 16146 Genova, Italy

²²INFN, Sezione di Roma Tor Vergata, 00133 Rome, Italy

²³INFN, Sezione di Torino, 10125 Torino, Italy

²⁴INFN, Sezione di Pavia, 27100 Pavia, Italy

²⁵Universit'e Paris-Saclay, CNRS/IN2P3, IJCLab, 91405 Orsay, France

²⁶Kyungpook National University, Daegu 41566, Republic of Korea

²⁷Mississippi State University, Mississippi State, MS 39762-5167

²⁸National Research Centre Kurchatov Institute - ITEP, Moscow, 117259, Russia

²⁹University of New Hampshire, Durham, New Hampshire 03824-3568

³⁰Norfolk State University, Norfolk, Virginia 23504

³¹Ohio University, Athens, Ohio 45701

³²Old Dominion University, Norfolk, Virginia 23529

³³University of Richmond, Richmond, Virginia 23173

³⁴Universita' di Roma Tor Vergata, 00133 Rome Italy

³⁵Skobeltsyn Institute of Nuclear Physics, Lomonosov Moscow State University, 119234 Moscow, Russia

³⁶University of South Carolina, Columbia, South Carolina 29208

³⁷Temple University, Philadelphia, PA 19122

³⁸Thomas Jefferson National Accelerator Facility, Newport News, Virginia 23606

³⁹Universidad Técnica Federico Santa María, Casilla 110-V Valparaíso, Chile

⁴⁰Università degli Studi dell'Insubria, 22100 Como, Italy

⁴¹Università degli Studi di Brescia, 25123 Brescia, Italy

⁴²University of Glasgow, Glasgow G12 8QQ, United Kingdom

⁴³Virginia Tech, Blacksburg, Virginia 24061-0435

⁴⁴University of Virginia, Charlottesville, Virginia 22901

⁴⁵College of William and Mary, Williamsburg, Virginia 23187-8795

⁴⁶Yerevan Physics Institute, 375036 Yerevan, Armenia

(Dated: March 9, 2020)

We report a measurement of a beam-target double-polarisation observable (E) for the $\bar{\gamma}\bar{n}(p) \rightarrow K^+\Sigma^-(p)$ reaction. The data were obtained impinging the circularly polarised energy-tagged photon beam of Hall B at Jefferson Lab on a longitudinally polarised frozen-spin hydrogen deuteride (HD) nuclear target. The E observable for an effective neutron target was determined for centre-of-mass energies $1.70 \leq W \leq 2.30$ GeV, with reaction products detected over a wide angular acceptance by the CLAS spectrometer. This new double-polarisation data gives unique constraints on the strange decays of excited neutron states. Inclusion of the new data within the Bonn-Gatchina theoretical model results in significant changes for the extracted photocouplings of a number of established nucleon resonances. Possible improvements in the PWA description of the experimental data with additional “missing” resonance states, including the $N(2120)^{3/2^-}$ resonance, are also quantified.

1. INTRODUCTION

A central aim of hadron spectroscopy is to obtain a deeper understanding of how bound quark systems form from their fundamental partonic degrees of freedom (the quarks and gluons). The properties of such bound quark systems reveal valuable information on the underlying dynamics and their structure, while providing an important challenge to quantum chromodynamics (QCD) and its ability to fully describe the non-perturbative phenomena underlying hadron structure [1]. Although the nucleon is probably the most abundant bound quark system in the universe, our understanding of its dynamics and structure remains elusive. Specifically, the nucleonic excitation spectra evaluated in QCD-based approaches (e.g. phenomenological constituent quark models [2–7], and lattice QCD [8–10]) predict many more excited states than currently established in experiment. Consequently, the “missing resonance” problem is an important focus for the world’s electromagnetic beam facilities with the aim of achieving a better understanding of the nucleon from QCD.

The excited nucleon spectrum is characterised by interfering, broad, and overlapping resonances for all but

the lowest mass states, making the determination of their properties (e.g. photocouplings, lifetimes, spins, parities, decay branches) challenging. The four complex amplitudes that determine the reaction dynamics at fixed kinematics [11] can be unambiguously determined from eight well-chosen combination of observables, referred to as a “complete” measurement¹. Therefore, kinematically (in W , and $\cos\theta$) complete and precise measurements of single- and double-polarisation observables utilising combinations of linearly and circularly polarised photon beams, transversely and longitudinally polarised targets, as well as the final state (recoiling) baryon polarimetry, in combination with partial wave analysis, are essential to resolve these states [11, 13, 17–19]. Furthermore, various resonances can have different photocouplings to neutron or proton targets [20, 21] and also differ in their preferred decay branches, necessitating data from a wide range of final states such as $N\pi$, $K\Lambda$, $K\Sigma$, multiple meson decays such as $N\pi\pi$, and even vector meson decays such as $N\omega$ [3, 11, 22]. In fact, constituent quark model calculations [3] indicate that a number of currently “missing” or poorly established states could have escaped experimental constraint because of a stronger decay coupling to the strange sector ($K\Lambda$ or $K\Sigma$) rather than the (comparatively) well studied πN . Recent double-polarisation measurements from proton targets in the strange-decay sector have been particularly successful in establishing new states [23–32]. Disappointingly, the current database of such reactions for neutron targets is sparse, with only a single double-polarisation measurement obtained for $K^0\Lambda$ and $K^0\Sigma^0$ final states [33], obtained with quite limited statistics. In this work we present the first measurement of the double-polarisation beam-target helicity

* nicholas@jlab.org

† Current address:Mississippi State University, Mississippi State, MS 39762-5167

‡ Current address:Université Paris-Saclay, CNRS/IN2P3, IJ-CLab, 91405 Orsay, France

§ Current address:University of York, York YO10 5DD, United Kingdom

¶ Current address:unused, unused

** Current address:Idaho State University, Pocatello, Idaho 83209

†† Current address:Università degli Studi di Brescia, 25123 Brescia, Italy

‡‡ Current address:University of Connecticut, Storrs, Connecticut 06269

¹ It has been established that due to data with finite error bars, a “complete” measurement that allows the unique determination of amplitudes is rather difficult [12–16].

135 asymmetry (E) for the reaction $\vec{\gamma}\vec{n} \rightarrow K^+\Sigma^-$, utilizing
 136 a circularly polarised tagged-photon beam and a longi-
 137 tudinally polarised hydrogen deuteride (HD) target, as
 138 an effective polarised-neutron target. The measurement
 139 is an important addition to the present world database
 140 for $K^+\Sigma^-$, which currently only comprises cross section
 141 determinations from CLAS [34, 35] and a measurement
 142 of a single-polarisation observable, the beam-spin asym-
 143 metry (Σ), measured in a restricted kinematic range at
 144 LEPS [31], and it provides important new constraints to
 145 the reaction mechanism.

146 The paper is organised as follows: after the short in-
 147 troduction, Section 1, Section 2 gives a description of the
 148 experimental setup, Section 3 introduces the polarisation
 149 observable E , and Section 4 gives an overview of the final
 150 state selection and the analysis procedure to extract E .
 151 In Section 5 the new E data are compared with current
 152 theoretical models and the implications for the neutron
 153 excited states is discussed.

154 2. EXPERIMENTAL SETUP

155 The experiment was conducted at the Thomas Jef-
 156 ferson National Accelerator Facility (JLab) utilising the
 157 Continuous Electron Beam Accelerator Facility (CE-
 158 BAF) and the CEBAF Large Acceptance Spectrometer
 159 (CLAS) [36] in Hall B (see Fig. 1). CLAS was a toroidal
 160 magnetic field analysing spectrometer covering polar an-
 161 gles between $\sim 8^\circ$ and 140° with large azimuthal accep-
 162 tance ($\sim 83\%$). The spectrometer also utilised a variety of
 163 tracking, time-of-flight, and calorimeter systems to pro-
 164 vide particle identification and 4-vector determination for
 165 particles produced in electro- or photo-induced reactions.
 166

167 The current data were obtained as part of the E06-
 168 101 experiment [37] (referred to as the g14 experiment),
 169 in which an energy-tagged polarised-photon beam,
 170 impinging on a 5-cm-long solid target of polarised hydrogen
 171 deuteride (HD) [38, 39] placed in the centre of CLAS.
 172 The energy-tagged (with energy resolution $\Delta E \sim 0.2\%$)
 173 and circularly-polarised photon beam was produced by
 174 impinging a longitudinally polarised electron beam on a
 175 thin gold radiator, with post-bremsstrahlung electrons
 176 momentum analysed in a magnetic tagging spectrome-
 177 ter [40]. The degree of photon polarisation was between
 178 20-85% depending on the incident photon energy, the
 179 electron-beam energy and the electron polarisation. The
 180 photon polarisation was determined using the Maximon
 181 and Olsen formula [41] utilising the energy of the incident
 182 and bremsstrahlung electrons, as well as the polarisa-
 183 tion of the incident electron beam, which was on average
 184 $P_e = 0.82 \pm 0.04$. This was periodically measured using
 185 the Hall B Møller polarimeter [42]. Information from the
 186 tagger spectrometer was used to identify and reconstruct
 187 the energy of the photon that initiated the reaction in
 188 CLAS.
 189

190 During the experiment, the polarisation of the photon

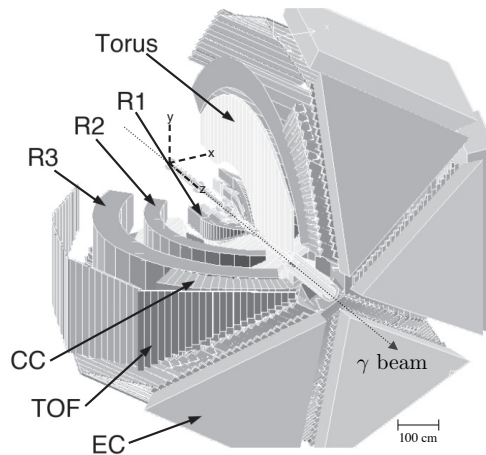


FIG. 1. A perspective view of CLAS showing the torus magnet, the three regions of drift chambers (R1–R3), the Cerenkov counters (CC), the time-of-flight detector (TOF), and the electromagnetic calorimeters (EC). The CLAS reference frame, also indicated here, was defined with the z axis along the beamline and the y axis perpendicular to the horizontal. Figure from Ref. [36].

beam was flipped pseudo-randomly with ~ 960 Hz flip rate between the two helicity states. The vector polarisation for deuterons (i.e. bound neutrons) within the HD target was between 23 – 26% and it was continuously monitored using nuclear magnetic resonance measurements [38]. An in-beam cryostat that produced a 0.9 T holding field operating at 50 mK was used to hold the target polarisation, achieving relaxation times of about a year. The orientation of the target polarisation was also periodically flipped between directions parallel or anti-parallel to the incoming photon beam. The flipping of the photon and target polarisations allowed the determination of E using asymmetries, as described below, that significantly suppressed systematic uncertainties related with the detector acceptance. For more details on the experimental setup for the g14 experiment, see Ref [33].

3. POLARISATION OBSERVABLE E

Measurements employing a circularly polarised photon beam in combination with a longitudinally polarised target give access to the double-polarisation observable E . The differential cross section for the $\vec{\gamma}\vec{n} \rightarrow K^+\Sigma^-$ reaction for the case of a polarised beam and target is given by [19, 43]:

$$\left(\frac{d\sigma}{d\Omega}\right) = \left(\frac{d\sigma}{d\Omega}\right)_0 (1 - P_T^{eff} P_\odot E), \quad (1)$$

where $\left(\frac{d\sigma}{d\Omega}\right)_0$ denotes the unpolarised differential cross section, P_T^{eff} denotes the effective target polarisation (accounting for events that originate from unpolarised

material within the target cell), and P_{\odot} the degree of circular photon polarisation². The observable E is extracted from asymmetries, A , in the reaction yields arising from different orientations of the beam and target polarisations:

$$A(W, \cos \theta_{K^+}^{cm}) = \frac{\left(\frac{d\sigma}{d\Omega}\right)^{\uparrow\downarrow} - \left(\frac{d\sigma}{d\Omega}\right)^{\uparrow\uparrow}}{\left(\frac{d\sigma}{d\Omega}\right)^{\uparrow\downarrow} + \left(\frac{d\sigma}{d\Omega}\right)^{\uparrow\uparrow}}, \quad (2)$$

where $\uparrow\uparrow$ and $\uparrow\downarrow$ denote a parallel or anti-parallel orientation of the photon and target polarisations, respectively. The polarisation observable E is then given by

$$E = \frac{1}{P_T^{eff} P_{\odot}} A(W, \cos \theta_{K^+}^{cm}). \quad (3)$$

This method allows the determination of E from the reaction yields for different combinations of the target-beam polarisations, while significantly reducing systematic effects from the detector acceptance.

4. DATA ANALYSIS

Events containing a single K^+ and a single π^- in the final state (without further restrictions on any additional neutral tracks), were selected to provide a sample of $\gamma n(p) \rightarrow K^+\Sigma^-(p)$, where the Σ^- has decayed to $n\pi^-$ (with 99.8% branching ratio). Particle identification and photon selection was done following standard procedures adopted for E06-106 analyses, as discussed in Refs. [33] and [44].

The $K^+\pi^-$ yield was further analysed to select the reaction of interest and remove unwanted backgrounds. Due to limitations in the separation of pions and kaons at high momenta in CLAS, a fraction of events from the $\pi\pi$ final state were present in our yield. These were removed using kinematical cuts³.

Further cuts were applied to the remaining event sample. The kaon missing mass ($MM_{\gamma n \rightarrow K^+X}$) and the $K^+\pi^-$ missing mass ($MM_{\gamma n \rightarrow K^+\pi^-X}$) were calculated assuming a free neutron target (the systematic effect on the determination of E using this assumption was investigated as discussed later in this Section), and these are plotted in a bi-dimensional histogram shown in

Fig. 2. Events from the reaction of interest lie where the $MM_{\gamma n \rightarrow K^+Y}$ corresponds to the nominal mass of the Σ^- and $MM_{\gamma n \rightarrow K^+\pi^-X}$ corresponds to the nominal mass of the neutron. The red lines in Fig. 2 indicate the two-dimensional cuts used to select the reaction of interest. The parameters of the two-dimensional cut were opti-

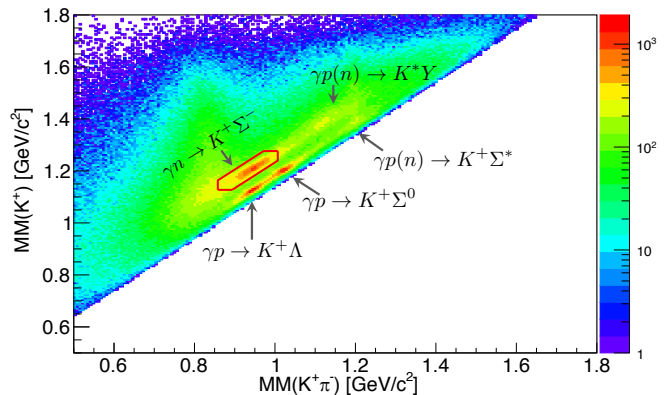


FIG. 2. Missing-mass distribution of $\gamma n \rightarrow K^+Y$ as a function of $\gamma n \rightarrow K^+\pi^-X$. The regions where the different reaction channels contribute are indicated by the arrows on the figure. The region enclosed by the red boundary contains the selected events.

mised to remove background contributions while maintaining a good event sample, as described below. Figure 2 indicates the background channels, such as $\gamma p \rightarrow K^+\Lambda$, $\gamma p \rightarrow K^+\Sigma^0$, $\gamma p(n) \rightarrow K^*Y$ and $\gamma p(n) \rightarrow K^+\Sigma^*$, which can potentially contribute to the $\gamma n \rightarrow K^+\Sigma^-$ yield. To quantify the contribution of background events to the event sample, a comprehensive list of reactions that included the above channels was simulated, processed through the CLAS acceptance and analysed identically to the $K^+\Sigma^-$ events. The final selection cuts applied to the data were optimised to reduce the background-to-total (B2T) ratio to the level of a few percent. With the tuned cuts (Fig. 2) the dominant background of $\gamma n \rightarrow K^+\Sigma^*$ was reduced to $B2T_{\gamma n \rightarrow K^+\Sigma^*} < 2\%$, while retaining a large fraction of the true yield. Contributions from $\gamma p(n) \rightarrow K^*Y$, were even smaller. The quantification of the background contributions allowed us to include their effects in the systematic uncertainty estimation.

Measurements with an empty-target cell (i.e. without the HD target material) were used to quantify the contribution to the yield of events originating from the aluminium cooling wires or entrance/exit windows. These events originated from unpolarised nucleons (i.e. are associated with $P_T = 0$) and account must be made for the resulting “dilution” of the target polarisation. This was calculated based on the ratio of empty-target to full-target data within z -vertex cuts (with z along the beamline) that define the target cell (see Fig. 1 in Ref. [33]). This dilution factor, D_F , was then utilised in the extraction of the helicity asymmetry from the data by using the effective target polarisation: $P_T^{eff} = D_F P_T$. Our studies have shown no statistically significant variation in the

² The full cross-section equation indicates that two additional polarisation observables, P and H , are also accessible by studying the angular dependence of the decay products of the hyperon (taking into account the analysing power of Σ^- , $\alpha = 0.068$). In this analysis, the observables P and H are integrated out.

³ For correctly identified events the missing mass of $\gamma n \rightarrow K^+\pi^-X$ reconstructs the neutron mass from the Σ^- decay. To establish the kaon-misidentified background events, which contribute only to events with kaon momenta above 1.2 GeV/c, the missing mass of $\gamma n \rightarrow \pi^+\pi^-Y$ was also calculated for each event, assuming the pion mass for the “kaon” track. Events with M_Y consistent with the nucleon mass were then removed as they result from the reaction $\gamma n \rightarrow \pi^+\pi^-n$

kinematic dependence of the dilution factor and thus an overall constant $D_F = 0.728 \pm 0.003$ was used.

A thorough assessment of systematic effects in the extracted (E) observable was carried out [45]. This included examining the effects of the applied particle identification cuts and reaction-vertex cuts (and therefore the effective target polarisation), as well as determining systematic uncertainties originating from the determination of the photon and target polarisation. Contributions from background channels were extensively investigated by varying the reaction-reconstruction cuts, and these were the major contributor to systematic uncertainty ($\Delta E_{background}^{syst} = 0.087$). Further, systematic uncertainties arising from the Fermi motion of the target nucleon were investigated utilising the correlation between the Fermi momentum and the missing-mass of $\gamma n \rightarrow K^+ \Sigma^-$. These were found to be small ($< 3\%$). No kinematic dependence of the systematic uncertainties was evident and therefore an upper estimate of a kinematic-independent uncertainty was established. The absolute systematic uncertainty associated with the determination of E was found to be $\Delta E^{syst} = 0.116$. In addition, a relative systematic scale uncertainty that stems from the target and photon polarisation, as well as the determination of the dilution factor, was estimated to be $\Delta E^{syst}/E = 6.9\%$.

5. RESULTS AND DISCUSSION

The measured beam-target polarisation observable E is presented in Fig. 3 for six centre-of-mass energy (W) bins between 1.7 and 2.3 GeV and for six bins in K^+ center-of-mass angle ($\theta_{K^+}^{cm}$). The centre-of-mass frame is calculated assuming the target neutron at rest. However, the effect of Fermi motion on the value of W is small compared to the bin widths. The reported W value for each E_γ bin (see figure) is obtained from the event-weighted mean of the E_γ distribution. The angular bins are contiguous and have varying widths in response to the angular variation in the reaction yield. The experimental data show a positive value of E for most of the sampled bins. As E must have a value of ± 1 at $\cos \theta_{K^+}^{cm} \rightarrow \pm 1$ to conserve angular momentum, values of E outside of our measured region must vary rapidly. The curves in Fig. 3 are the predictions of the E observable from the Kaon-MAID-2000 [46] (dashed green), Kaon-Maid-2017 [47] (dotted magenta) and Bonn-Gatchina-2017 [48] (solid black) PWA models. It is clear that the models give rather divergent predictions for this observable, and none of the current solutions give consistent agreement with the experimental data over the sampled kinematic range. This suggests that the relevant photoproduction amplitudes are not well constrained by the current world-data, and that the new data have the potential to provide new information. The Bonn-Gatchina-2017 [48] solution is fitted to the entire database of meson photoproduction from the nucleon. In this solution the only direct $K^+ \Sigma^-$ constraints in the database are from

the cross section determination [34, 35].

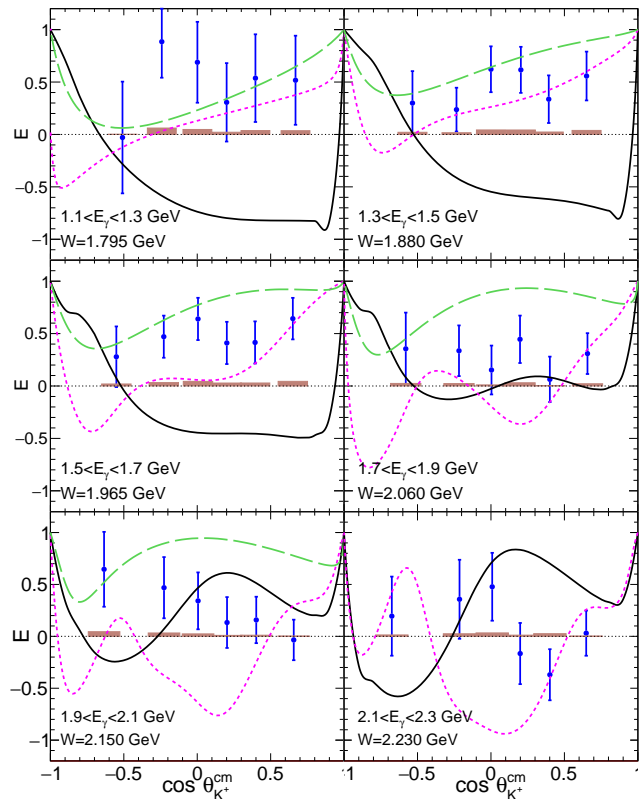


FIG. 3. Angular dependence of the determined beam-target double-polarisation observable E (with error bars indicating the combined statistical and absolute systematic uncertainties; the bar chart shows the magnitude of the systematic scale uncertainty) for the six center-of-mass energy W bins compared with the Kaon MAID 2000 (dashed green) and 2017 (dotted magenta), as well as predictions from Bonn-Gatchina (solid black). The event-weighted W value and the photon-energy bin are indicated in the panels.

In Fig. 4 the impact of including the new data in the Bonn-Gatchina database is explored. The predictions of E from the new fits (Bonn-Gatchina-2019) are shown by the dashed red lines and blue dotted lines⁴. It is seen that the new solution gives a much improved fit to the data (for comparison, the Bonn-Gatchina-2017 solution is repeated on this figure (solid black line)). The implications of the new Bonn-Gatchina-2019 fit for the properties of the excited states are shown in Table I, where the helicity couplings calculated at the pole position are compared with previously published values [49]. In the new solution, the phase of the coupling residues – defined by the interference of the resonance with other contributions including non-resonance terms and tails from other

⁴ Note that the new fit also included the beam asymmetry data in very forward kaon kinematics from LEPS [31] which was not included in the previous Bonn-Gatchina-2017 fit.

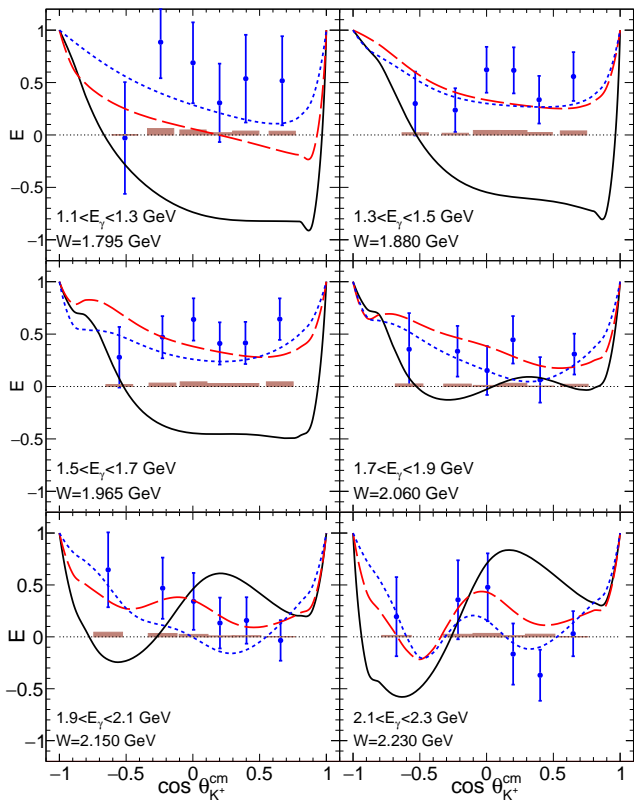


FIG. 4. The new Bonn-Gatchina description of the helicity asymmetry data. The error bars reflect the total statistical and absolute systematic uncertainty, whereas the bar chart reflects the scale systematic uncertainty. The Bonn-Gatchina-2017 solution [48] is shown with the solid black curves. The solutions with the new data on the helicity asymmetry included in the fit is shown with the dashed red lines. The solution with added D_{13} state is shown with the dotted blue lines.

states – between the $L_{IJ}^{K\Sigma} = S_{11}$ and P_{13} partial waves has changed substantially from earlier fits. In fact, this is now better constrained by data since the E observable allows separation of the helicity projections 1/2 and 3/2 (corresponding to projections of the S_{11} and P_{13} , respectively). As a result the new data produces significant changes in the extracted photocouplings of the individual states, particularly the $N(1720)^{3/2+}$ and $N(1900)^{3/2+}$ as indicated in Table I.

The helicity 1/2 coupling of the $N(1720)^{3/2+}$ state has the same magnitude as before but is rotated in phase by 90° , while the corresponding helicity coupling of the $N(1900)^{3/2+}$ state has decreased by almost a factor 2. This results in a different behavior of the $N(1720)^{3/2+}$ 1/2 helicity amplitude whose interference with the S_{11} partial wave defines the behavior of the E observable. The 3/2 helicity coupling of $N(1720)^{3/2+}$ notably decreases and is rotated by 85° while the 3/2 helicity coupling of the $N(1900)^{3/2+}$ state did not exhibit significant changes.

TABLE I. The $\gamma n N^*$ helicity couplings of nucleon states ($\text{GeV}^{-1/2} 10^{-3}$) expressed in terms of the transverse helicity amplitudes and calculated as residues in the pole position. Previously reported values [49] are indicated in parentheses. Only resonances, which either are most important for the description of the new data or deviate by more than one standard deviation from the published results, are included.

	$A_{1/2}^n$	Phase	$A_{3/2}^n$	Phase
$N(1895)^{1/2-}$	-20 ± 7 (-15 ± 10)	$50 \pm 20^\circ$ ($60 \pm 25^\circ$)		
$N(1720)^{3/2+}$	-45 ± 15 (-25^{+40}_{-15})	$20 \pm 30^\circ$ ($-75 \pm 35^\circ$)	-35 ± 20 (100 ± 35)	$-15 \pm 30^\circ$ ($-80 \pm 35^\circ$)
$N(1900)^{3/2+}$	-45 ± 15 (-98 ± 20)	$-5 \pm 20^\circ$ ($-13 \pm 20^\circ$)	80 ± 12 (74 ± 15)	$0 \pm 20^\circ$ ($5 \pm 15^\circ$)

Furthermore, the new Bonn-Gatchina-201 [50] solution seems to better describe the sparse cross section data at backward angles for specific kinematic bins. This is clearly indicated by the red dashed lines in the lower left panel of Fig. 5. Specifically, a different $K\Sigma$ cross section at backward kaon angles is now suggested, which is generally consistent with the available data in this region. The improved agreement of the new solution with the existing beam asymmetry data from LEPS [31] for $K\Sigma$ is also presented in Fig. 5.

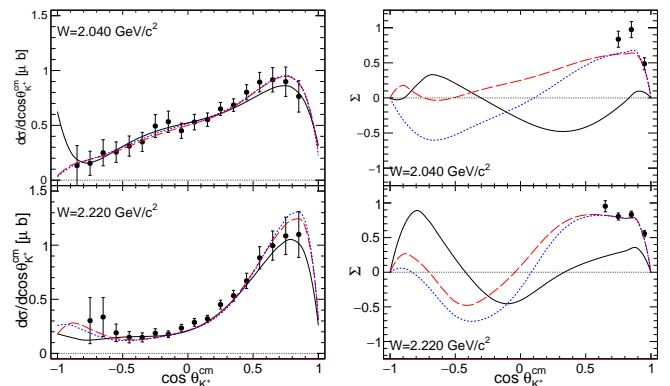


FIG. 5. The description of the differential cross section (data from [34]) (left) and the beam asymmetry (data from [31]) (right). The Bonn-Gatchina-2017 solution [48] is shown with the solid black curves. The solutions that includes the new data on the helicity asymmetry is shown with the dashed red lines, whereas the solution with an added D_{13} state is shown with the dotted blue lines.

The sensitivity of the new E data to missing or poorly established excited states was also explored within the Bonn-Gatchina framework. The database for reactions off neutron targets is much smaller than for the proton, so there is the potential to gain new sensitivities with the current data. There is significant current interest to gain sensitivity to the $N(2120)^{3/2-}$, a resonance predicted by many theoretical models of nucleon structure but still escaping proper experimental confirmation. The Bonn-Gatchina fits were repeated with the inclusion of

additional states, one at a time, with varying properties (e.g. helicity couplings). The best description of the new data was obtained when adding a D_{13} resonance of mass 2170 MeV. The results of this new fit (Bonn-Gatchina 2019-2) are shown by the dashed blue lines in Figs. 4 and 5. The new E data are consistent with such a D_{13} contribution, which results in improved fits for many of the sampled W and K^+ $c.m.$ angle ranges. However, the level of improvement in the description of the E observable is not sufficient to make strong claims. The new solution does however provide a basis to explore sensitivities in other observables. The D_{13} has a strong predicted influence on the beam asymmetry and future measurements over a wider angular range could provide valuable constraints on its existence (e.g. see Fig. 5). Other possibilities were also explored. The inclusion of a missing ($N(2060)^{5/2^-}$) marginally improved the agreement with data, particularly in the last energy bin, but was slightly worse in the bin which included the resonance central mass value. Furthermore, no improvement was obtained by including missing states with positive parity.

6. SUMMARY

We present the first measurement of a double polarisation beam-target observable (E) for the reaction $\gamma n \rightarrow K^+\Sigma^-$, utilizing a circularly polarised photon beam and spin-polarised HD as an effective neutron target. The new E data is an important addition to the sparse world database constraining the strange decays of excited neutron states. Model predictions for the E observable in this channel were strongly divergent and none gave a good description of the new data over the

full kinematic range. Fitting the new data in the framework of one of the models (Bonn-Gatchina) resulted in new constraints in the interference of the S_{11} and P_{13} partial waves, and significant changes in the extracted photocoupling of a number of resonance states, including the $N(1720)^{3/2^+}$, $N(1895)^{1/2^-}$, and $N(1900)^{3/2^+}$. Improved fits to the new E data could be obtained with the inclusion of a “missing” D_{13} resonance, although further measurements are clearly necessary to better establish this state. The determination of the beam spin asymmetry, Σ , for the reaction $\gamma n(p) \rightarrow K^+\Sigma^-(p)$ at backward angles could provide the necessary constraints for further investigations of this excited state.

7. ACKNOWLEDGMENTS

This work has been supported by the U.K. STFC (ST/P004385/1, ST/P004008/1, and ST/L00478X/1) grants as well as by the RSF16-12-10267 grant. We also acknowledge the outstanding efforts of the staff of the Accelerator and Physics Divisions at Jefferson Lab that made this experiment possible. The Southeastern Universities Research Association (SURA) operated the Thomas Jefferson National Accelerator Facility for the United States Department of Energy under contract DE-AC05-06OR23177. Further support was provided by the National Science Foundation, the United Kingdom’s Science and Technology Facilities Council, the Italian Istituto Nazionale di Fisica Nucleare, the Chilean Comisión Nacional de Investigación Científica y Tecnológica (CONICYT), the French Centre National de la Recherche Scientifique, the French Commissariat à l’Energie Atomique, and the National Research Foundation of Korea.

-
- [1] I. G. Aznauryan *et al.*, *Int. J. Mod. Phys. E* **22**, 1330015 (2013).
- [2] S. Capstick and W. Roberts, *Prog. Part. Nucl. Phys.* **45**, 241 (2000).
- [3] S. Capstick and W. Roberts, *Phys. Rev. D* **58**, 074011 (1998).
- [4] S. Capstick and N. Isgur, *Phys. Rev. D* **34**, 2809 (1986).
- [5] U. Löring, B. Metsch, and H. Petry, *Eur. Phys. J. A* **10**, 395 (2001).
- [6] L. Y. Glozman, W. Plessas, K. Varga, and R. F. Wagenbrunn, *Phys. Rev. D* **58**, 094030 (1998).
- [7] M. M. Giannini, E. Santopinto, and A. Vassallo, *Eur. Phys. J. A* **12**, 447 (2001).
- [8] R. G. Edwards, J. J. Dudek, D. G. Richards, and S. J. Wallace, *Phys. Rev. D* **84**, 074508 (2011).
- [9] J. Dudek and R. Edwards, *Phys. Rev. D* **85**, 054016 (2012).
- [10] R. G. Edwards, N. Mathur, D. G. Richards, and S. J. Wallace, *Phys. Rev. D* **87**, 054506 (2013).
- [11] W.-T. Chiang and F. Tabakin, *Phys. Rev. C* **55**, 2054 (1997).
- [12] T. Vrancx, J. Ryckebusch, T. Van Cuyck, and P. Vancraeyveld, *Phys. Rev. C* **87**, 055205 (2013).
- [13] J. Nys, J. Ryckebusch, D. G. Ireland, and D. I. Glazier, *Phys. Lett. B* **759**, 260 (2016).
- [14] D. G. Ireland, *Phys. Rev. C* **82**, 025204 (2010).
- [15] Y. Wunderlich, R. Beck, and L. Tiator, *Phys. Rev. C* **89**, 055203 (2014).
- [16] L. Tiator, “Complete experiments for pion photoproduction,” (2012), arXiv:1211.3927 [nucl-th].
- [17] C. G. Fasano, F. Tabakin, and B. Saghai, *Phys. Rev. C* **46**, 2430 (1992).
- [18] G. Keaton and R. Workman, *Phys. Rev. C* **54**, 1437 (1996).
- [19] A. M. Sandorfi, S. Hoblit, H. Kamano, and T. S. H. Lee, *J. Phys. G* **38**, 053001 (2011).
- [20] A. M. Sandorfi and S. Hoblit, *Nucl. Phys. A* **914**, 538 (2013).
- [21] T. Mart, C. Bennhold, and C. E. Hyde-Wright, *Phys. Rev. C* **51**, 1074(R) (1995).
- [22] S. Capstick and W. Roberts, *Phys. Rev. D* **57**, 4301 (1998).
- [23] K. H. Glander *et al.*, *Eur. Phys. J. A* **19**, 251 (2004).

- 510 [24] R. Castelijn *et al.*, Eur. Phys. J. A **35**, 39 (2008). 529
- 511 [25] M. Nanova *et al.*, Eur. Phys. J. A **35**, 333 (2008). 530
- 512 [26] R. Bradford *et al.*, Phys. Rev. C **73**, 035202 (2006). 531
- 513 [27] M. E. McCracken *et al.*, Phys. Rev. C **81**, 025201 (2010). 532
- 514 [28] M. Sumihama *et al.*, Phys. Rev. C **73**, 035214 (2006). 533
- 515 [29] J. W. C. McNabb *et al.*, Phys. Rev. C **69**, 042201 (2004). 534
- 516 [30] A. Lleres *et al.*, Eur. Phys. J. A **31**, 79 (2007). 535
- 517 [31] H. Kohriet *et al.*, Phys. Rev. Lett. **97**, 082003 (2006). 536
- 518 [32] C. A. Paterson, Phys. Rev. C **93**, 065201 (2016). 537
- 519 [33] D. Ho *et al.*, Phys. Rev. C **98**, 045205 (2018). 538
- 520 [34] S. A. Pereira *et al.*, Phys. Lett. B **688**, 289 (2010). 539
- 521 [35] N. Compton *et al.*, Phys. Rev. C **96**, 065201 (2017). 540
- 522 [36] B. A. Mecking *et al.*, Nucl. Instrum. Meth. A **503**, 513 (2003). 541
- 523 (2003). 542
- 524 [37] K. Ardashev *et al.*, JLab Proposal PR06-101 www.jlab.org/exp_prog/proposals/06/PR06-101.pdf. 543
- 525 [prg/exp_prog/proposals/06/PR06-101.pdf](http://www.jlab.org/exp_prog/proposals/06/PR06-101.pdf). 544
- 526 [38] M. Lowry *et al.*, Nucl. Instr. Meth. A **815**, 31 (2016). 545
- 527 [39] C. D. Bass *et al.*, Nucl. Instrum. Meth. A **737**, 107 (2014).
- 528 [40] D. I. Sober *et al.*, Nucl. Instrum. Meth. A **440**, 263 (2000).
- [41] H. Olsen and L. Maximon, Phys. Rev **114**, 887 (1959).
- [42] J. M. Grames *et al.*, Phys. Rev. ST Accel. Beams **7**, 042802 (2004).
- [43] I. S. Barker, A. Donnachie, and J. K. Storrow, Nucl. Phys. B **95**, 347 (1975).
- [44] D. Ho *et al.*, Phys. Rev. Lett **118**, 242002 (2017).
- [45] J. Flemings, Ph.D. Thesis, University of Edinburgh (2016).
- [46] T. Mart and C. Bennhold, Phys. Rev. C **61**, 012201 (1999).
- [47] T. Mart, AIP Conference Proceedings **1862**, 020001 (2017).
- [48] A. V. Anisovich *et al.*, Phys. Lett. B **772**, 247 (2017).
- [49] A. V. Anisovich *et al.*, Phys. Rev. C **96**, 055202 (2017).
- [50] A. Sarantsev, Personal Communication (2019).